

1
2
3
4
5
6
7
8
9
10
11
12
13
14
15
16
17
18
19
20
21
22
23
24

Processes controlling $\delta^7\text{Li}$ in rivers illuminated by study of streams and groundwaters draining basalts

Xiao-Ming Liu^{1,2*}, Christoph Wanner³, Roberta L. Rudnick¹, and William F. McDonough¹

- 1. Department of Geology, University of Maryland-College Park, College Park, MD, USA
- 2. Geophysical Lab, Carnegie Institute of Washington, Washington D.C., USA
- 3. Earth Sciences Division, Lawrence Berkeley National Laboratory, Berkeley, CA, USA

*Corresponding author contact information:
Geophysical Lab
Carnegie Institute of Washington
5251 Broad Branch Rd. NW,
Washington, DC 20015-1305, USA
Tel: (301) 825-6841
Fax: (202) 478-8901
Email: xliu@gl.ciw.edu

Word count for the main text is 6599, 8 Figures and 2 Tables

25 **Abstract**

26 We evaluate the factors influencing the abundance, [Li], and isotopic composition of
27 riverine Li delivered to the oceans through analyses and modeling of [Li] and $\delta^7\text{Li}$ in streams and
28 groundwaters draining a single continental lithology, the Columbia River Basalts (CRBs). The
29 streams were sampled in different climate zones that lie east (dry), and west (wet) of the
30 Cascades Mountains, and during two different seasons (summer and late winter) in order to
31 evaluate climatic and seasonal influences on Li isotopes in rivers. Dissolved Li ($\delta^7\text{Li}_{\text{dis}} = +9.3$ to
32 $+30.4$) is systematically heavier than that of fresh or weathered CRBs (-4.7 to $+6.0$, Liu et al.,
33 2013, *GCA* 115, 73-91), suspended loads (-5.9 to -0.3), and shallow groundwaters ($+6.7$ to $+9.4$),
34 consistent with previous studies showing that Li isotope fractionation is affected by equilibration
35 between stream water and secondary minerals. However, the lack of correlation between $\delta^7\text{Li}_{\text{dis}}$
36 and climate zone, the uniform secondary minerals and bedrock, coupled with the highly variable
37 ($>20\%$) $\delta^7\text{Li}_{\text{dis}}$ indicate that other factors exert a strong control on $\delta^7\text{Li}_{\text{dis}}$. In particular, the
38 heavier Li in streams compared to the shallow groundwaters that feed them indicates that
39 continued isotopic fractionation between stream water and suspended and/or bed loads has a
40 major influence on riverine $\delta^7\text{Li}$. Seasonal $\delta^7\text{Li}$ variation is observed only for streams west of the
41 Cascades, where the difference in precipitation rate between the dry and wet seasons is greatest.
42 Reactive transport model simulations reveal that riverine $\delta^7\text{Li}$ is strongly controlled by
43 subsurface residence times and the Li isotope fractionation occurring within rivers. The latter
44 explains why there is no positive correlation between $\delta^7\text{Li}$ and traditional weathering proxies
45 such as Si or normalized Si in rivers, as riverine Li isotope fractionation drives $\delta^7\text{Li}$ to higher
46 values during transport, whereas the concentrations of major cations and anions are diluted. The
47 varying residence time for groundwaters feeding the western streams in summer (long residence
48 times, higher $\delta^7\text{Li}$, greater weathering) and winter (short residence times, lower $\delta^7\text{Li}$, less
49 weathering) explains the observed seasonal variations. A global, negative correlation between
50 $\delta^7\text{Li}$ and Li/Na for streams and rivers draining basaltic catchments reflects the overall transport
51 time, hence the amount of silicate weathering. Based on our results, the increase of $\delta^7\text{Li}$ in
52 seawater during the Cenozoic is unlikely related to changing climate, but may reflect mountain
53 building giving rise to increased silicate weathering.

54

55 **Keywords:** lithium isotopes; chemical weathering; rivers and groundwaters, reactive transport
56 modeling

57

58 ***1. Introduction***

59 Chemical weathering of silicate rocks on Earth's surface plays a critical role in regulating
60 the global carbon cycle over geological time-scales (e.g., Berner et al., 1983). Basalt weathering,
61 in particular, may significantly contribute to the global silicate weathering flux. For example,
62 Gaillardet et al. (1999), suggested a minimum of 25% of the silicate weathering flux to the
63 oceans derives from weathering of basalt. Attempts to illuminate chemical weathering processes
64 using natural samples generally take two approaches: studies of river waters (e.g., Dessert et al.,
65 2001; Gaillardet et al., 1999), and studies of weathering profiles or weathered regoliths (e.g.,
66 Brimhall et al., 1991; Nesbitt and Wilson, 1992). River chemistry is able to provide rate-related
67 constraints, such as chemical weathering fluxes and CO₂ consumption rates (Gaillardet et al.,
68 1999), although only for the present.

69 Li isotopes can potentially provide insights into the weathering flux from the continents
70 over time (Liu and Rudnick, 2011), and changing climate, if the changes in $\delta^7\text{Li}$ in the seawater
71 record (Misra and Froelich, 2012) can be deciphered. The Li isotopic composition in seawater is
72 a function of the input of rivers and hydrothermal fluid, and the output into secondary minerals
73 formed via low temperature basalt alteration and sediment clay authigenesis (referred to as
74 "reverse weathering") (Chan et al., 1992). The dramatic (8‰) increase in $\delta^7\text{Li}$ in seawater
75 through the Cenozoic has been interpreted to reflect the changing composition of riverine inputs
76 that, in turn, reflect climatic and tectonic influences on continental weathering (Misra and
77 Froelich, 2012). Assuming a constant hydrothermal input, the significant increase in $\delta^7\text{Li}$
78 through the Cenozoic may indicate increases in the riverine input (a greater flux and/or higher
79 $\delta^7\text{Li}$), an increased output flux of low $\delta^7\text{Li}$, or both. Therefore, understanding the controls on
80 riverine Li isotopes is a first-order requirement for understanding the secular evolution of
81 seawater.

82 Li is contained mainly in silicates and is released, with attendant isotopic fractionation,
83 during weathering (e.g., Huh et al., 2001; 1998; Kısakürek et al., 2005; 2004; Rudnick et al.,

84 2004). Lithium's two stable isotopes, ^7Li and ^6Li , have great fractionation potential due to their
85 17% mass difference. Differences in Li isotopic composition are expressed as $\delta^7\text{Li}$ (‰) =
86 $([^7\text{Li}/^6\text{Li}]_{\text{sample}} / [^7\text{Li}/^6\text{Li}]_{\text{standard}} - 1) \times 1000$, where the standard used is a lithium carbonate, L-SVEC
87 (Flesch et al., 1973). Lithium is a water-soluble trace element, but neither primary basalt
88 dissolution nor metamorphic dehydration appear to cause significant Li isotopic fractionation
89 (Marschall et al., 2007; Pistiner and Henderson, 2003; Qiu et al., 2011a; 2011b; 2009; Teng et
90 al., 2007; Wimpenny et al., 2010a). By contrast, Li isotopes fractionate significantly during
91 incongruent continental weathering, due to the formation of secondary minerals, such as clays
92 (e.g., Huh et al., 1998; Kiskakürek et al., 2004; Pistiner and Henderson, 2003; Pogge von
93 Strandmann et al., 2006; Rudnick et al., 2004; Teng et al., 2004). Lithium has a few more
94 advantages as a potential geochemical tracer of weathering. Li has only one redox state (+1
95 charge), and is thus insensitive to changes in oxygen fugacity compared to Fe, Cr, Cu, Mo, etc.
96 In addition, Li is not a nutrient, so its elemental and isotopic behavior is not directly influenced
97 by biological processes (e.g., Lemarchand et al., 2010). Finally, Li is enriched in silicates and
98 depleted in carbonates, so its abundance and isotopic composition in rivers mainly reflect
99 continental silicate weathering (one caveat is that riverine Li can be significantly influenced by
100 the presence of evaporites, e.g., Huh et al., 1998).

101 Studies investigating the use of $\delta^7\text{Li}$ as a weathering proxy (Huh et al., 2001; 1998; Millot et al.,
102 2010; Pogge von Strandmann et al., 2006; Vigier et al., 2009) have not fully discerned why the
103 Li isotope composition of rivers does not show consistent correlation with certain silicate
104 weathering proxies. For instance, Huh et al. (1998) did not observe a clear correlation between
105 $\delta^7\text{Li}_{\text{dis}}$ and $^{87}\text{Sr}/^{86}\text{Sr}$, $\delta^7\text{Li}_{\text{dis}}$ and $[\text{Li}]$ (using square brackets around elements to indicate
106 concentration) as well as between $\delta^7\text{Li}_{\text{dis}}$ and Si/TZ^+ (Total cation charge, $\text{TZ}^+ =$
107 $\text{Na}^+ + 2\text{Mg}^{2+} + \text{K}^+ + 2\text{Ca}^{2+}$ in 10^{-3} equivalents per liter, mEq/L) when compiling global river data. By
108 contrast, for the Orinoco drainage basin a strong inverse correlation was observed between
109 $\delta^7\text{Li}_{\text{dis}}$ and $^{87}\text{Sr}/^{86}\text{Sr}$ as well as between $\delta^7\text{Li}_{\text{dis}}$ and Si/TZ^+ (Huh et al., 2001). In addition, in some
110 studies a correlation between $\delta^7\text{Li}$ and chemical weathering rates (in mass/area/time) was
111 observed (Vigier et al., 2009), whereas in others no clear relationship could be identified (Millot
112 et al., 2010). The lack of consistent correlation may reflect variations in climate (e.g., tropical vs.
113 temperate climates), lithologies, hydrology, and sampling seasons encompassed in previous river

114 studies. Here we seek to illuminate the causes of Li isotopic fractionation produced during
115 weathering by studying surface waters draining a single lithology (basalt) as a function of
116 climate, season, and groundwater residence time. The Columbia River Basalts (CRBs) afford this
117 opportunity due to their large areal extent, which encompasses different climate zones and allows
118 sampling within a single lithology having limited isotopic variability. Understanding the
119 processes that control $\delta^7\text{Li}_{\text{dis}}$ will, in turn, afford greater insight into the changing $\delta^7\text{Li}$ observed
120 in seawater with time.

121

122 ***2. Geological setting, climate and samples***

123 The geological setting of the sampling area is described in Liu et al. (2013) and a brief
124 account is provided here. The CRBs are continental flood basalts that erupted during the
125 Miocene (between 17 Ma to 6 Ma) in the US Pacific Northwest, covering large parts of southern
126 Washington, northeastern Oregon and parts of western Idaho (Fig. 1).

127 The CRBs crop out both east and west of the Cascade Mountain Range. The Cascades
128 developed progressively from subduction zone magmatism since the Late Eocene, with
129 topography increasing more or less steadily since the Late Oligocene (Kohn et al., 2002 and
130 references therein). The mountains created two different climate zones that affected the CRBs
131 via the rain shadow effect; regions west of the Cascades have high mean annual precipitation
132 (MAP) (1500-2000 mm), whereas annual precipitation east of the Cascades is less than 300 mm
133 (Kohn et al., 2002; Takeuchi et al., 2010). In addition, the monthly precipitation rates vary more
134 in the west, where the mean monthly precipitation rate during the wet season (October-May) is
135 up to 10 times greater than that during the dry season (June to September) (Fig. A1). By contrast,
136 differences in monthly precipitation rates east of the Cascades are usually less than a factor of 2.

137 The advantages of studying streams and groundwaters in this area include: 1) The streams
138 only drain a single lithology, the CRBs. 2) Sampling streams from different climate zones allows
139 investigation of how annual precipitation rates, and thus climate, may have influenced riverine Li
140 isotopic composition. 3) Due to the variable seasonal precipitation (Fig. A1), sampling in two
141 seasons allow us to assess the effect of seasonally variable precipitation rates and corresponding
142 variable surface runoff (Fig. A2) on Li isotopic compositions. 4) Sampling of groundwaters that

143 are the potential sources of the streams allows distinction between Li isotope fractionation
144 occurring in aquifers compared to fractionation occurring in rivers.

145

146 *3. Samples and analytical methods*

147 *3.1 Sampling*

148 Dissolved and suspended load samples from 10 CRB streams were collected in July
149 2010, and again in March 2012 to study possible seasonal variations; samples from the mouths of
150 the much larger Deschutes and John Day rivers, which have lithologically diverse catchments,
151 were also taken for comparison. In addition, five groundwater samples were collected in March
152 2012, as well as an additional stream (Mosquito Creek, R11) (Fig. 1).

153 At each site, pH, temperature, electrical conductivity, and total dissolved solids (TDS)
154 were measured using a multi-meter (Hanna® Instruments) with analytical accuracy of ± 0.05 , \pm
155 0.5°C , $\pm 2\%$ $\mu\text{S}/\text{cm}$, and $\pm 2\%$ ppm, respectively. All stream water samples were obtained using
156 a peristaltic pump and filtered using a 142 mm filter holder system with $0.2\ \mu\text{m}$ cellulose acetate
157 filters. Filtered waters were collected in pre-cleaned Nalgene® bottles. Filters were placed in air-
158 tight Ziploc plastic bags for transport back to the lab. The suspended loads of the stream waters
159 were recovered from the filters in the clean lab. The sample tubing was pumped dry after each
160 sample collection and one liter of deionized water was pumped through the system to clean it
161 between each sampling event. At the start of sampling at a new site, a liter of sample water was
162 first collected into the pre-cleaned bottles and then discarded. Finally, about two liters of water
163 were collected, acidified using five drops (~ 0.25 ml) of concentrated HCl and stored in
164 Nalgene® bottles for transport to the lab. Following this procedure, two 125 ml pre-cleaned
165 Nalgene® bottles were filled with water for anion (without acidification) and major and trace
166 cation analyses (acidified using two drops of ~ 0.1 ml concentrated HCl).

167 Groundwaters were sampled either from existing pumping systems that tap into deep-
168 seated aquifers or faucets fed by shallow wells. The sampling method outlined above for streams
169 was also used for the groundwaters (Table 2). One groundwater sample (G4, Lind) was taken
170 from a new municipal well in the town of Lind, WA, which taps into an aquifer buried 220 m

171 below ground and is estimated to be >50 ka old based on radiocarbon age dating (T. Tolan,
172 personal communication). A second groundwater sample (G1, Spring Creek) was collected at the
173 Spring Creek National Fish Hatchery from an aquifer ~ 200 m deep, containing little or no
174 modern water and having an overall age of thousands of years (Hinkle, 1996). Thus, these two
175 groundwaters are unlikely to be the sources of waters in the streams.

176 ***3.2 Major and trace elements in dissolved loads***

177 Major and trace cations in dissolved loads were analyzed using an Element 2 single
178 collector Inductively Coupled Plasma-Mass Spectrometer (ICP-MS) at the University of
179 Maryland. Calibration curves were created using pure element solutions (Alfa Aesar[®]) and
180 standard and water samples were doped with the same amount of indium to correct for
181 instrumental drift ([In] = 2 ppb). The accuracy and precision of the analyses were determined by
182 repeat analyses of the international river standard SLRS-5, with accuracy of cations assessed at
183 better than 4% (n = 11 for SLRS-5), except for K (<10%), based on its certified value (Table
184 A.1).

185 Major anion concentrations were measured by ion chromatography in the
186 Biogeochemical Lab at the University of Maryland. Anion concentrations were measured using a
187 Dionex ICS-1500 ion chromatograph, equipped with an AS14 4-mm analytical column and a
188 guard column. An eluent of 3.5 mM of Na₂CO₃ with 1.0 mM NaHCO₃ was used at a flow rate of
189 0.3 mL/min. The detection limits of the ion chromatograph are 0.01 mg/L, 0.01 mg NO₃/L and
190 0.02 mg SO₄/L for Cl⁻, NO₃⁻ and SO₄²⁻, respectively. The accuracy of the analyses are better than
191 ~5% based on repeat analyses of standards (see Table A.2). HCO₃⁻ concentrations were
192 estimated based on charge balance.

193 ***3.3 Lithium isotope analyses***

194 All sample preparation and analyses were performed in the Geochemical Laboratory at
195 the University of Maryland. A description of sample dissolution, column chemistry, analytical
196 blanks and instrumental analysis is provided in the electronic appendix (Text A1). Long-term
197 precision is better than ± 1‰ (2 σ); several USGS rock standards were run repeatedly during the
198 course of this study (Table A.3). BHVO-1 yielded δ⁷Li of +4.6 ± 1.0 (n= 5) cf. 4.0 to 5.6 in the
199 literature (GeoReM database: <http://georem.mpch-mainz.gwdg.de/>); BCR-2 yielded δ⁷Li of +2.9

200 ± 1.5 (n = 3) cf. 2.6 to 4.6 in the literature (GeoReM database); and AGV-1 yielded $\delta^7\text{Li}$ of +5.2
201 ± 0.6 (n = 3) cf. 4.6 and 6.7 for AGV-1 in Liu et al. (2010) and Magna et al. (2004), respectively.

202 **3.3.1 Handling of dissolved loads**

203 Approximately 30 ml to 2 L of filtered stream and groundwaters (depending on the
204 volume collected) were first weighed and then evaporated in large Savillex® Teflon beakers
205 (160 ml) or Teflon evaporation dishes (400 ml) on a hot plate ($T < 100^\circ\text{C}$). A 3:1 mixture of HF-
206 HNO_3 was added to the samples, which were then transferred into screw-top Savillex® Teflon
207 beakers (15ml) placed onto a hot plate ($T < 120^\circ\text{C}$) for an overnight dissolution followed by an
208 evaporation step. The sample was then treated with concentrated HNO_3 and HCl until all solids
209 were dissolved and the final solutions were clear. The final dried sample was picked up in 4 N
210 HCl for column separation.

211 **3.3.2 Dissolution of suspended loads**

212 Suspended load samples were washed off the filters into large Savillex® Teflon beakers
213 (160 ml) using Milli-Q water and then transferred into screw-top Teflon beakers and dried on a
214 hot plate ($T < 70^\circ\text{C}$). The dried samples were then scraped off the beaker and weighed into clean
215 Teflon beakers; sample sizes ranged from several milligrams to tens of milligrams. The samples
216 were then dissolved using a 3:1 mixture of HF and HNO_3 in a screw-top Teflon beaker on a hot
217 plate ($T \approx 90^\circ\text{C}$), dried, then pickup up by HNO_3 and HCl addition until all solids were dissolved
218 and the final solutions were clear. The final dried sample was dissolved in 4 N HCl for column
219 separation.

220 **3.4 Reactive transport modeling**

221 In order to investigate the influence of silicate weathering on $\delta^7\text{Li}_{\text{dis}}$, a series of
222 thermodynamically- and kinetically-controlled reactive transport model simulations were carried
223 out using the code TOUGHREACT V2 (Xu et al., 2011). TOUGHREACT has been used to
224 evaluate isotopic fractionation coupled to water-rock interaction and hydrological processes in a
225 variety of subsurface environments and laboratory experiments (eg., Singleton et al., 2005;
226 Sonnenthal et al., 1998; Wanner and Sonnenthal, 2013). Each modeled scenario is composed of
227 two individual simulations to model silicate weathering and associated Li isotope fractionation (i)

228 during subsurface flow and (ii) within rivers (Fig. 2). The model setup is closely related to the
229 simulations performed by Wanner et al. (2014) modeling Li isotope fractionation associated with
230 granite weathering. Accordingly, only a short model description is provided below. Input
231 parameters and specific code capabilities used to simulate Li isotope fractionations are described
232 in detail in the electronic appendix (Text A2).

233 *3.4.1 Subsurface simulations*

234 Reactive transport along a basaltic subsurface was simulated for a fully saturated, 100 m
235 long porous media having a porosity of 10%, the porosity previously used to simulate Columbia
236 River Basalt weathering (Taylor and Lasaga, 1999). Fracture flow, the presence of highly porous
237 flow tops, as well as the unsaturated zone, were not incorporated into the model because our
238 focus is on assessing the sensitivity (i.e., trends) of dissolved $\delta^7\text{Li}$ values as a function of
239 residence time (i.e., amount of weathering), rather than on simulating detailed flow features of
240 actual unsaturated zones feeding aquifers and streams. Subsurface simulations were run for an
241 average linear groundwater flow velocity of 1 m/d to simulate a system dominated by advection.

242 Pure water in equilibrium with atmospheric CO_2 was specified as the initial and boundary
243 fluid compositions. A starting mineralogical composition similar to the normative mineralogy
244 reported for different Columbia River Basalt members (BVSP, 1981) (e.g., plagioclase, pyroxene,
245 olivine, glass) was assigned to the solid part of the porous medium (see Tables A.4 and A.5 for
246 mineral stoichiometries, corresponding thermodynamic and kinetic parameters and specified
247 initial and boundary conditions). Simulations were run for two different initial bulk Li
248 concentrations of 4 and 20 ppm, encompassing most of the range of [Li] observed in fresh CRB
249 (Liu et al., 2013), and to assess whether the initial Li concentration influences riverine $\delta^7\text{Li}$
250 values.

251 Because Li is moderately incompatible during igneous differentiation (Brenan et al.,
252 1998), Li is assumed to be mostly contained within a glassy basalt matrix and is introduced into
253 the model from a Li-bearing volcanic glass phase tabulated in the THERMODEM database
254 (Blanc et al., 2012). Li-bearing hematite and kaolinite were allowed to precipitate. It should be

255 noted that kaolinite and hematite are likely not the only secondary minerals forming, but they
256 serve as representatives for any other potentially precipitating Fe- and Al-bearing minerals.

257 To simulate the fate of individual Li isotopes, ^6Li and ^7Li were incorporated into the
258 mineral stoichiometries of primary Li-bearing volcanic glass, and secondary kaolinite and
259 hematite. An initial $\delta^7\text{Li}$ value of +1 was assumed for Li-bearing glass, which corresponds to the
260 average $\delta^7\text{Li}$ value measured for two different CRBs members (Liu et al., 2013). Similar to the
261 model of Bouchez et al. (2013), we do not distinguish between Li exchange-, Li surface
262 complexation-, or Li substitution reactions and Li uptake by secondary minerals and associated
263 Li isotopic fractionation is solely simulated during Li incorporation into precipitating kaolinite
264 and hematite. Li bearing secondary mineral precipitation is simulated by means of a solid
265 solution approach, such as described in detail by Wanner et al. (2014), as well as in the Text A2.
266 A fractionation factor ($\Delta^7\text{Li}_{\text{2ndMin-solution}} = \delta^7\text{Li}_{\text{2ndMin}} - \delta^7\text{Li}_{\text{solution}}$) of -10‰ was assigned for hematite
267 and kaolinite precipitation, which is within the range of Li isotope fractionation factors reported
268 or inferred for secondary mineral precipitation (Huh et al., 2001; Kısakürek et al., 2005; Pistiner
269 and Henderson, 2003; Pogge von Strandmann, 2006; 2010; Vigier et al., 2008; Zhang et al.,
270 1998). An extended discussion of fractionation factors can be found in the Text A2.

271 **3.4.2 River simulations**

272 River simulations were conducted essentially as batch simulations, where the flow
273 velocity was set to zero. In doing so, it was assumed that the reactive suspended load (i.e., solid
274 phase) is transported at the same velocity as the river water, which is in agreement with current
275 knowledge about the transport of suspended river loads (Fryirs and Brierley, 2013).

276 Two grid blocks were defined to simulate groundwater exfiltrating into river systems,
277 which is diluted by river water that previously experienced less water-rock interaction processes.
278 By setting the interfacial area (A_{inter} , Fig. 2) between the two grid blocks to 7000 m^2 , the Li
279 concentration of the exfiltrating groundwater was diluted by a factor of ~ 10 during a simulated
280 river residence time of 20 days, roughly corresponding to the Li concentration difference
281 observed between streams and groundwaters (Tables 1, 2). Reactions between the suspended

282 river load and river waters were only considered for the grid block initially containing
283 exfiltrating groundwater.

284 The suspended river load was assigned the same initial mineralogical composition as the
285 subsurface (Table A.5), assuming that this load contains a significant amount of primary silicate
286 minerals in addition to the dominant clays and oxides (Gaillardet et al., 1999). This model
287 assumption is consistent with Bouchez et al. (2011) who observed that the mineralogical
288 composition of the suspended load is dependent on the particle size and that primary silicate
289 minerals (e.g., feldspar) are enriched in the coarser fraction. Consequently, Li isotope
290 fractionation in the simulated river is assumed to occur in the same fashion as in the subsurface
291 simulations.

292 **4. Results**

293 Data for field measurements (pH, temperature, electrical conductivity, and TDS), major
294 and trace elements, in addition to Li isotopic data are given in Tables 1 and 2, for streams and
295 groundwaters, respectively. A comparison between summer and late winter data is shown in
296 Figs. A3 and A4 for field parameters and selected dissolved species, respectively.

297 **4.1 Field measurements**

298 Streams sampled in July 2010 display a temperature range from 13 to 22°C with pH
299 ranging from 7.2 to 8.7, while the streams sampled in March 2012 are cooler (1 to 9°C), but have
300 a similar range in pH (6.7 to 8.3). Groundwaters are warmer (10 to 29°C), and have higher pH
301 (7.7 to 9.6), compared to the streams sampled at the same time of the year (March). TDS in
302 streams east of the Cascades do not show significant seasonal variations (32 to 154 mg/L in July,
303 and 25 to 158 mg/L in March, Table 1) with the exception of Silva creek, where TDS varies by a
304 factor of two between seasons (64 in summer vs. 33 ppm in winter). By contrast, TDS in the
305 three streams west of the Cascades differ by up to a factor two between seasons (7-18 mg/L in
306 July, 10-32 mg/L in March). Groundwaters range to higher TDS values (90 to 253 mg/L, Table
307 2). The maximum TDS value was measured in a meromictic lake (i.e., a stratified lake that does
308 not mix between layers), the TDS of which exceeded the range of the multi-meter.

309 *4.2 Major elements*

310 Major cations and anions in stream water and groundwater samples are plotted using a
311 classic Piper Diagram (Piper, 1953), a trilinear diagram consisting of two equilateral triangles for
312 cations and anions, respectively, which are projected onto a central diamond (Fig. 3). In the
313 lower triangles, the points are expressed as a percentage of the total amount of cations or anions
314 in milliequivalents per liter. River and groundwaters are plotted in Fig. 3a and 3b for summer
315 and winter, respectively. River waters have clustered cation patterns in both summer and winter
316 illustrating that the water chemistry is inherited from a single lithology. Three shallow
317 groundwaters plot within the same domain as the streams, while two deep groundwaters (G1:
318 Spring Creek, and G4: Lind) show very different cation and anion patterns. Major elements such
319 as Na, Si and Ca, correlate with Mg, and hence with each other (Fig. A5). Similarly, the total
320 cation charge, TZ^+ ($TZ^+ = Na^+ + 2Mg^{2+} + K^+ + 2Ca^{2+}$ in 10^{-3} equivalents per liter, mEq/L), also
321 correlates ($R^2 = 0.98$) with [Mg] in stream waters. Groundwaters, except for the two deep
322 groundwaters (G1: Spring Creek, and G4: Lind), follow the same major element correlation, but
323 with higher concentrations. The sample from Silva Creek taken in July, 2010, has much higher
324 [Cl⁻] (54 mg/L) and [SO₄²⁻] (39 mg/L), compared to the other streams studied here and natural
325 streams elsewhere (where [Cl⁻] and [SO₄²⁻] are typically less than 10 mg/L), indicating that this
326 creek may have been subjected to anthropogenic contamination in the summer months (e.g.,
327 fertilizers).

328 Major cations in streams show very little variation between summer and winter; however,
329 anions show large variations (Fig. 3). Although little variation is observed for cation ratios,
330 actual concentrations (e.g., Si, Mg, and Na) tend to be slightly higher during the summer
331 sampling campaign (Table 1, Fig. A4). This observation corresponds well with pH values and
332 TDS concentrations, which were also slightly larger during the summer sampling campaign
333 (Table 1, Fig. A3). In the case of [Si] and TDS, the seasonal concentration increase is most
334 prominent in the western streams, with an increase of up to a factor two. By contrast, in the
335 eastern streams both concentration variations ([Si] and TDS) were significantly smaller, by a
336 factor less than ~1.3 (Table 1). In addition, although there is some seasonal variation of anion
337 concentrations among streams, the overall pattern likely reflects a mixture of water sources,

338 since all streams and shallow groundwaters plot along a straight line; the two deep groundwaters
339 fall off the trend in the upper diamond plot (Fig. 3).

340 **4.3 Li elemental and isotopic data**

341 The Li concentrations of dissolved loads vary from 0.2 to 4.7 $\mu\text{g/L}$ for both sampling
342 seasons. For individual streams, there is little difference in [Li] between the two sampling
343 campaigns (Table 1, Fig. 4), where [Li] shows a weak positive correlation with [Mg] ($R^2 = 0.7$)
344 and [Si] ($R^2 = 0.4$). $\delta^7\text{Li}_{\text{dis}}$ ranges from +10 to +30 in the streams sampled during the summer,
345 and shows a similar range in the streams sampled in the late winter (+9 to +22). In streams east
346 of the Cascades, $\delta^7\text{Li}_{\text{dis}}$ does not change with season, except for Silva Creek (+30 vs. +14‰),
347 which may reflect anthropogenic contamination, based on the high contents of $[\text{Cl}^-]$ and $[\text{SO}_4^{2-}]$.
348 A previous study has shown that anthropogenically contaminated groundwaters may show very
349 heavy $\delta^7\text{Li}$ values (up to $\sim +1000\text{‰}$), due to the use of heavy Li-enriched fertilizer (Négre et al.,
350 2010). By contrast, the streams to the west of the Cascades show consistently higher $\delta^7\text{Li}$ values
351 in the summer compared to the winter (Fig. 5).

352 Varying from 2 to 21 $\mu\text{g/L}$ (Table 1), groundwater [Li] is significantly higher than in the
353 streams. Moreover, with the exception of the two groundwaters from deep wells (shown as open
354 triangles in the figures), [Li] in groundwaters show similar correlations with [Si], but not with
355 [Mg], as seen in stream waters (Fig. 4). Except for the deep-seated Lind well water (G4,
356 +21.4‰), groundwater $\delta^7\text{Li}$ ($\delta^7\text{Li}_{\text{GW}}$) are between +6.7 and +9.4‰, which is on the very low end
357 of observed $\delta^7\text{Li}_{\text{dis}}$ (Tables 1, 2).

358 [Li] in the suspended loads varies from 7 to 24 $\mu\text{g/g}$ in the streams sampled during the
359 summer, and shows a greater range in the streams sampled during the late winter (from 13 to 66
360 $\mu\text{g/g}$). The $\delta^7\text{Li}$ of the suspended load ($\delta^7\text{Li}_{\text{sus}}$) is generally the same from season to season,
361 except for the Dechutes River, which shows a large change in $\delta^7\text{Li}_{\text{sus}}$ according to season (+4.2
362 in summer to -0.3 in late winter). With the exception of the summer Deschutes River sample,
363 $\delta^7\text{Li}_{\text{sus}}$ are lower compared to the average $\delta^7\text{Li}$ measured in fresh CRBs ($\delta^7\text{Li} = 1.1$, Liu et al.,
364 2013). The low $\delta^7\text{Li}_{\text{sus}}$ are comparable to the lower than average $\delta^7\text{Li}$ observed in weathered
365 CRB ($\delta^7\text{Li} = -5$ to 0) and the upper continental crust ($\delta^7\text{Li} = 0$ on average, Teng et al., (2004)).

366 **4.4 Simulation results**

367 **4.4.1 [Li] and $\delta^7\text{Li}$**

368 Simulated steady-state [Li] and [Si] profiles along our model domain (subsurface + river),
369 as well as corresponding $\delta^7\text{Li}$ profiles (i.e., $\delta^7\text{Li}_{\text{dis}}$, $\delta^7\text{Li}_{2\text{ndMin}}$ and $\delta^7\text{Li}_{\text{bulk-rock}}$) are shown in Figs.
370 6a and 6b for two different parental basalt Li concentrations of 4 and 20 ppm. Increasing [Li] in
371 basalt yields larger dissolved Li concentrations for a specific subsurface residence time (Fig. 6a),
372 but does not change $\delta^7\text{Li}$ values, as illustrated by superimposing $\delta^7\text{Li}_{\text{dis}}$ vs. residence time
373 behavior (Fig. 6b). These results thus imply that subsurface and riverine $\delta^7\text{Li}$ values are not
374 sensitive to the Li concentrations of the parent rock, nor to the subsequent variable riverine [Li].
375 This simulation result is supported by a lack of correlation observed between $\delta^7\text{Li}_{\text{dis}}$ and [Li]
376 (Table 1).

377 The $\delta^7\text{Li}_{\text{dis}}$ and $\delta^7\text{Li}_{2\text{ndMin}}$ values steadily increase with increasing subsurface and/or
378 riverine residence time in the model (Fig. 6b). The slope of the $\delta^7\text{Li}$ increase with time is
379 dependent on the specified fractionation factor. For a lower fractionation factor (i.e., less
380 fractionation), longer residence time is needed to reach the same $\delta^7\text{Li}$ as for $\Delta^7\text{Li} = -10\%$, or vice
381 versa. However, the pattern of increasing $\delta^7\text{Li}$ with increasing residence time is not sensitive to
382 the specified fractionation factor. The $\delta^7\text{Li}_{\text{dis}}$ increases seen along the model domain are
383 produced by our solid solution approach (Wanner et al., 2014), ensuring that [Li] in precipitating
384 hematite and kaolinite increases with increasing [Li]. This assumption is consistent with an
385 experimental study showing that [Li] in synthesized smectite increases linearly with aqueous [Li]
386 (Decarreau et al., 2012). Because the dissolution rate of the parent rock remains constant (Table
387 A.4), the ratio between Li that is incorporated into hematite and kaolinite, and the Li being
388 released from the parent rock increases with increasing residence time, thus, continuously
389 driving $\delta^7\text{Li}_{\text{dis}}$ and $\delta^7\text{Li}_{2\text{ndMin}}$ to higher values. The Li isotopic composition of the bulk rock is not
390 changed (Fig. 6b) because the amount of secondary minerals formed during the 100 years for
391 which the simulation were run were too low to drive the bulk rock $\delta^7\text{Li}$ to lower values. In
392 contrast to $\delta^7\text{Li}_{\text{dis}}$ and $\delta^7\text{Li}_{2\text{ndMin}}$, aqueous [Li] and [Si] decrease (Fig. 6a) due to dilution when
393 water flowing along the subsurface exfiltrates into the river.

394 **4.4.2 Weathering proxies**

395 Simulated profiles for silicate weathering proxies such as [Si], normalized Si (Si/TZ^+),
396 [Li], normalized Li (Li/TZ^+), and Li/Na that have been previously used to constrain silicate
397 weathering intensity (e.g., Huh et al., 2001; 1998; Millot et al., 2010; Pogge von Strandmann et
398 al., 2010; 2006) are shown in Fig. 6c. These profiles reflect a proxy's ideal behavior, because
399 processes potentially affecting the use of a specific weathering proxy (e.g., biological activity,
400 anthropogenic contamination, salt leaching) were not considered in our simulations.

401 A negative correlation between $\delta^7\text{Li}_{\text{dis}}$ and Li/Na (Fig. 6c) reflects Li incorporation into
402 hematite and kaolinite, whereas Na remains in solution. Accordingly, although [Li] also
403 increases with residence time in the subsurface, the Li/Na ratio's decrease with increasing
404 residence time is due to Li incorporation into these secondary minerals. Other weathering proxies
405 show a distinct correlation with $\delta^7\text{Li}_{\text{dis}}$ only within a specific model domain (subsurface vs. river).
406 In particular, concentration proxies such as [Si] and [Li] are positively correlated with $\delta^7\text{Li}_{\text{dis}}$
407 along the subsurface domain, but once exfiltrated, the correlations change sign because Li
408 isotope fractionation is ongoing, whereas aqueous species concentrations decrease due to mixing
409 with more superficial (i.e., meteoric) water.

410 **5. Discussion**

411 The observation that riverine $\delta^7\text{Li}_{\text{dis}}$ (+9 to +30) is systematically higher than $\delta^7\text{Li}$ values
412 of the corresponding suspended loads ($\delta^7\text{Li}_{\text{sus}} = -6$ to 0), as well as fresh and weathered CRBs
413 ($\delta^7\text{Li} = -5$ to +5, Liu et al., 2013), confirms that high $\delta^7\text{Li}_{\text{dis}}$ is mainly generated by Li isotope
414 fractionation occurring during basalt weathering (e.g., Huh et al., 2001; 1998; Pogge von
415 Strandmann et al., 2010; 2006).

416 The most striking observation from our measurements, however, is the large variation in
417 $\delta^7\text{Li}_{\text{dis}}$ (about 20‰ in summer, and > 10‰ in late winter) covering almost the entire range of
418 $\delta^7\text{Li}$ (+6 to +32) reported in major world rivers (Huh et al., 1998). This observation is especially
419 remarkable because we sampled only small streams and groundwaters within the CRBs, for
420 which catchment lithological differences are small. Some previous studies attribute large $\delta^7\text{Li}_{\text{dis}}$
421 variations to formation of different secondary minerals that have different fractionation factors
422 with water (Millot et al., 2010; Wimpenny et al., 2010b). However, we see no evidence that the
423 large $\delta^7\text{Li}_{\text{dis}}$ variations in our study are due to the presence of different Li-bearing secondary

424 minerals, as saturation index (SI) calculations (Fig. A7) and studies of weathering profiles (Liu et
425 al. 2013) suggest that all of the streams and groundwaters are saturated with the same secondary
426 mineral assemblage (hematite, kaolinite and gibbsite). We therefore postulate that factors other
427 than mineralogical differences (i.e., primary and secondary Li bearing phases) have a major
428 control on the Li isotopic composition of the streams.

429 *5.1 Residence time*

430 The rise of $\delta^7\text{Li}$ with increasing residence time seen in the simulation (Fig. 6b) implies
431 that subsurface residence time in particular, and the hydrological cycle in general have major
432 controls on $\delta^7\text{Li}_{\text{dis}}$. In fact, in a plot of $\delta^7\text{Li}_{\text{dis}}$ vs. Li/Na, our sample observations fall between the
433 two curves defined by the minimum and maximum simulated bulk rock [Li] (Fig. 6d). We infer
434 that the Li/Na ratio is an excellent proxy for residence time, because [Na] is at least three orders
435 of magnitude higher than [Li] (Tables 1 and 2) and thus is not as strongly affected by small
436 amounts of secondary mineral precipitation. However, Li/Na is also affected by the bulk rock
437 concentration and the slope of the $\delta^7\text{Li}_{\text{dis}}$ vs. Li/Na correlation seems to be a function of the bulk
438 rock [Li], whereas the location along a particular correlation (i.e., the measured $\delta^7\text{Li}_{\text{dis}}$ value)
439 defines the residence time (Fig. 6d).

440 Significant seasonal precipitation variations are only observed for areas west of the
441 Cascades (Fig. A.1). Since precipitation rates have a primary control on the hydrological cycle,
442 this observation suggests that western streams are characterized by a more seasonally variable
443 subsurface residence time distribution, whereas eastern streams show a less variable residence
444 time distribution. Accordingly, the strong control of $\delta^7\text{Li}_{\text{dis}}$ by residence time accounts for the
445 seasonal $\delta^7\text{Li}_{\text{dis}}$ variations observed in streams west of the Cascades and the lack of variations
446 seen in eastern streams (Tables 1, 2).

447 The increase in $\delta^7\text{Li}_{\text{dis}}$ seen with an increasing river to subsurface residence time ratio
448 (Fig. 6b) also explains why riverine $\delta^7\text{Li}_{\text{dis}}$ is generally greater than groundwater $\delta^7\text{Li}_{\text{dis}}$ (Fig. 7
449 and Tables 1 and 2). Accordingly, our observations and simulation results support the hypothesis
450 that suspended river loads are reactive due to the presence of fine-grained primary silicate
451 mineral particles, and therefore continued Li isotope fractionation is occurring within streams.

452 This is also supported by a recent study of Lemarchand et al. (2010), who found $\delta^7\text{Li}_{\text{dis}}$ in
453 streams draining a granitic catchment to be significantly greater than that of springs feeding these
454 streams.

455 *5.2 Climate control*

456 There is no clear distinction in $\delta^7\text{Li}_{\text{dis}}$ values between western and eastern streams,
457 suggesting that the amount of annual precipitation, and thus climatic conditions, do not have a
458 direct influence on $\delta^7\text{Li}$. This lack of climatic influence is consistent with the results of Millot et
459 al. (2010), who suggested that neither mean annual precipitation nor distance to the coast have an
460 influence on $\delta^7\text{Li}_{\text{dis}}$ in waters from the Mackenzie River basin. In addition, despite the large
461 temperature difference between summer and late winter ($\sim 10^\circ\text{C}$), there is no change in riverine
462 $\delta^7\text{Li}_{\text{dis}}$ in eastern streams.

463 Interestingly, as discussed in the previous section, a clear seasonal control on $\delta^7\text{Li}_{\text{dis}}$ was
464 observed for streams west of the Cascades (Fig. 5), which is probably related to the large
465 seasonal difference in monthly precipitation observed there (Fig. A1). The proposal that average
466 subsurface residence time is longer during drier periods is in good agreement with significantly
467 larger TDS and [Si] observed for western streams during the summer compared to the winter
468 (Table 1). A correlation between subsurface residence times and aqueous concentrations, and
469 thus TDS, is expected because longer residence times allow for increased mineral dissolution and
470 exchange (Fig. 6). Overall, climate indirectly affects $\delta^7\text{Li}$ as precipitation rates control the
471 hydrological cycle and thus residence time distributions. However, $\delta^7\text{Li}$ is a poor proxy for
472 climate because many other parameters affect the hydrological cycle as well (e.g., mountain
473 building, pCO_2 , temperature, vegetation).

474 *5.3 $\delta^7\text{Li}$ as a tracer of chemical weathering*

475 This study has illuminated the factors that control Li isotopic fractionation in the
476 dissolved loads of rivers ($\delta^7\text{Li}_{\text{dis}}$). Li isotopic fractionation in rivers is caused by fractionation
477 between solution and secondary minerals (e.g., Huh et al., 2001; 1998; Pogge von Strandmann et
478 al., 2010; 2006), and it has been suggested that the large variability in $\delta^7\text{Li}_{\text{dis}}$ may be partially
479 caused by different fractionation factors associated with Fe-Mn oxyhydroxides in places without
480 soils or clays (Millot et al., 2010; Wimpenny et al., 2010b). Our study shows that $\delta^7\text{Li}_{\text{dis}}$ is not

481 simply controlled by mineral-specific fractionation, as there is no correlation between $\delta^7\text{Li}_{\text{dis}}$ and
482 SI of the oversaturated secondary minerals, such as hematite and kaolinite (Fig. A7). We have
483 shown that parameters such as reservoir residence time and reaction between suspended and
484 dissolved loads in rivers can significantly influence $\delta^7\text{Li}_{\text{dis}}$, given a constant fractionation factor
485 between solution and secondary minerals (Fig. 6), and there is no need (or evidence) to call upon
486 variable fractionation factors related to the dominance of different secondary to explain variable
487 $\delta^7\text{Li}_{\text{dis}}$ in rivers.

488 Our simulations (Fig. 6) agree very well with observations (Fig. 7), as we see a clear
489 negative correlation between $\delta^7\text{Li}_{\text{dis}}$ and the Li/Na ratio, whereas, $\delta^7\text{Li}_{\text{dis}}$ does not correlate with
490 [Si] or Si/TZ⁺, and shows only a weak negative correlation with Li/TZ⁺ (Fig. 6c). Based on our
491 simulations and data, we infer that, with the exception of Li/Na, $\delta^7\text{Li}_{\text{dis}}$ and various silicate
492 weathering proxies based on elemental concentrations (e.g., [Li], [Si], TZ⁺) are only correlated
493 when a natural system is dominated by either Li isotope fractionation occurring in the subsurface
494 (in which case there is a positive correlation between $\delta^7\text{Li}_{\text{dis}}$ and the weathering proxies), or
495 occurring in rivers (in which case there is a negative correlation between $\delta^7\text{Li}_{\text{dis}}$ and the proxies).
496 If Li isotope fractionation occurs in both settings, there will be no correlation, as seen in our
497 results. This finding may explain why correlations between $\delta^7\text{Li}_{\text{dis}}$ and concentration proxies are
498 observed in some studies (e.g., Huh et al., 2001; Pogge von Strandmann et al., 2010), but not in
499 others (this study; Millot et al., 2010).

500 Overall, this study also has implications for using Li isotopes as tracers of chemical
501 weathering in rivers, and consequently, in seawater through time. In previous studies, multiple
502 weathering proxies, such as [Si] and Si/TZ⁺, [Li], combined with Li isotopes (e.g., Huh et al.,
503 2001; 1998; Pogge von Strandmann et al., 2006), have been used to try to constrain silicate
504 weathering intensity. However, correlations between $\delta^7\text{Li}_{\text{dis}}$ and these proxies may be produced
505 or destroyed due to the effects we simulated, such as the residence time in the subsurface (as
506 suggested in Millot et al., 2010), Li isotope fractionation and mineral dissolution in rivers. Our
507 study suggests that $\delta^7\text{Li}_{\text{dis}}$ is more robust than other tracers of silicate weathering, because it is
508 linked to the degree of water-rock interactions along a specific flow path (e.g., in the subsurface
509 and in rivers). In general, the larger the $\delta^7\text{Li}_{\text{dis}}$ in a specific river, the more water-rock
510 interactions (primary mineral dissolution + secondary mineral precipitations) have occurred such

511 as shown by Wanner et al. (2014). We demonstrate that, in rivers draining single lithology
512 catchments, $\delta^7\text{Li}_{\text{dis}}$ is negatively correlated with Li/Na, suggesting that the combined $\delta^7\text{Li}_{\text{dis}}$ vs.
513 Li/Na plot (Fig. 7d) may be a sensitive indicator of the extent of chemical weathering occurring
514 in streams and groundwater reservoirs. Moreover, this finding is observed globally by clear
515 negative correlations between $\delta^7\text{Li}_{\text{dis}}$ vs. Li/Na for river waters worldwide that drain only or
516 mainly basalts (Fig. 8). The global correlations observed in Fig. 8 is well related to our
517 simulations (Fig. 6d), where we show that a perfect correlation is only observed for constant
518 basalt [Li], which is clearly not the case when comparing basalts from the world over (e.g., [Li]
519 = 3 to 23 ppm in fresh CRBs).

520 Finally, $\delta^7\text{Li}_{\text{dis}}$ is influenced by many hydrological parameters, so it is not straightforward
521 to use $\delta^7\text{Li}_{\text{dis}}$ as a silicate weathering tracer in terms of interpreting secular evolution of riverine
522 inputs to seawater. For example, for very fast flow at a high discharge, the overall silicate
523 weathering rate (in moles/year) is very high. However, the $\delta^7\text{Li}$ value should remain low because
524 of the short residence time. Assuming the rise in $\delta^7\text{Li}$ in seawater in the past 60 Ma (Misra and
525 Froelich, 2012) is due primarily to changing riverine input with minor effects of discharge
526 variations (Wanner et al., 2014), our work suggests that this signature reflects increased silicate
527 weathering rates on the continents, which may or may not be directly related to changing climate
528 (as we see no direct correlation between $\delta^7\text{Li}_{\text{dis}}$ and climate), but could well be due to tectonic
529 uplift that causes an increase in water-rock reaction.

530

531 **6. Conclusions**

532 The main conclusions from this study are:

- 533 1. Large $\delta^7\text{Li}_{\text{dis}}$ variations (up to 20‰) are observed in streams that only drain basalts,
534 suggesting that Li isotopic compositions in streams are controlled by factors other
535 than the lithology of their catchments.
- 536 2. $\delta^7\text{Li}_{\text{dis}}$ is significantly higher than $\delta^7\text{Li}$ of groundwaters, suggesting that Li isotope
537 fractionation occurring in rivers themselves play a major role on riverine $\delta^7\text{Li}_{\text{dis}}$.

- 538 3. A lack of direct correlation between climatic conditions (i.e., mean annual
539 precipitation, temperature) and riverine $\delta^7\text{Li}_{\text{dis}}$, and correlations between seasonal
540 precipitation variations and $\delta^7\text{Li}_{\text{dis}}$ suggest that subsurface residence times strongly
541 influence riverine $\delta^7\text{Li}_{\text{dis}}$.
- 542 4. Model simulations of reactive transport with variable residence times show that Li
543 isotope fractionation occurs in both the subsurface and in rivers, causing many
544 traditional silicate weathering proxies (e.g., [Si], Si/TZ+) to show no, or only a weak
545 correlation with $\delta^7\text{Li}_{\text{dis}}$.
- 546 5. $\delta^7\text{Li}_{\text{dis}}$ and Li/Na in dissolved loads of rivers are only sensitive to the amount of
547 water-rock interaction over time and are, thus, useful tracers of the degree of silicate
548 chemical weathering occurring in single lithology catchments.
- 549 6. If the increase in $\delta^7\text{Li}$ in seawater through the Cenozoic is due primarily to changing
550 riverine input, our results suggest that the increase may be uniquely related to tectonic
551 uplift, which causes increased weathering due to the increase in denudation and the
552 decreasing weathering intensity. Climatic controls on chemical weathering are
553 apparently not as important.

554 *Acknowledgements*

555 We thank Richard Ash for assistance with the ICP-MS/MC-ICP-MS analyses, Igor
556 Puchtel for help in the clean lab, Shuiwang Duan and Tammy Newcomer for major anion
557 analyses, Terry Tolan for sampling guidance and discussion, Marshall Gannett, Steve Hinkle,
558 Steve Cox, and Mike Free for help with fieldwork logistics, and Christie Galen for
559 accompanying up in the field and showing us great birds. Sujay Kaushal kindly provided access
560 to his Biogeochemistry laboratory and provided guidance on water sampling. We are grateful for
561 discussions and comments from Jerome Gaillardet and Cin-Ty Lee. The manuscript benefited
562 greatly from the review comments of three anonymous reviewers. Jean Lynch-Stieglitz is also
563 thanked for her editorial handling and constructive comments. This work was supported by a
564 grant from the National Science Foundation (EAR 0948549 to RLR and WFM) and an Ann G.
565 Wylie Dissertation Fellowship awarded to X-ML from the University of Maryland. X-ML
566 acknowledges postdoctoral fellowship support from the Carnegie Institution of Washington. CW
567 was supported by the U.S. Department of Energy, Geothermal Technologies Program, Energy
568 Efficiency and Renewable Energy Office, Award No GT-480010-12.

References

- Basaltic Volcanism Study Project (1981). Basaltic Volcanism on the Terrestrial Planets. Pergamon Press, Inc., New York. 1286 pp.
- Berner, R.A., Lasaga, A.C., Garrels, R.M., 1983. The carbonate-silicate geochemical cycle and its effect on atmospheric carbon-dioxide over the past 100 million years. *American Journal of Science* 283, 641-683.
- Blanc, P., Lassin, A., Piantone, P., Azaroual, M., Jacquemet, N., Fabbri, A., Gaucher, E.C., 2012. Thermoddem: A geochemical database focused on low temperature water/rock interactions and waste materials. *Applied Geochemistry* 27, 2107-2116.
- Bouchez, J., Gaillardet, J., France-Lanord, C., Maurice, L., Dutra-Maia, P., 2011. Grain size control of river suspended sediment geochemistry: Clues from Amazon River depth profiles. *Geochemistry Geophysics Geosystems* 12.
- Bouchez, J., von Blanckenburg, F., Schuessler, J.A., 2013. Modeling novel stable isotope ratios in the weathering zone. *American Journal of Science* 313, 267-308.
- Brenan, J.M., Neroda, E., Lundstrom, C.C., Shaw, H.F., Ryerson, F.J., Phinney, D.L., 1998. Behaviour of boron, beryllium, and lithium during melting and crystallization: Constraints from mineral-melt partitioning experiments. *Geochimica et Cosmochimica Acta* 62, 2129-2141.
- Brimhall, G.H., Lewis, C.J., Ford, C., Bratt, J., Taylor, G., Warin, O., 1991. Quantitative geochemical approach to pedogenesis - Importance of parent material reduction, volumetric expansion, and eolian influx in lateralization. *Geoderma* 51, 51-91.
- Decarreau, A., Vigier, N., Pálková, H., Petit, S., Vieillard, P., Fontaine, C., 2012. Partitioning of lithium between smectite and solution: An experimental approach. *Geochimica et Cosmochimica Acta* 85, 314-325.
- Dessert, C., Dupré, B., Francois, L.M., Schott, J., Gaillardet, J., Chakrapani, G., Bajpai, S., 2001. Erosion of Deccan Traps determined by river geochemistry: impact on the global climate and the $^{87}\text{Sr}/^{86}\text{Sr}$ ratio of seawater. *Earth and Planetary Science Letters* 188, 459-474.
- Flesch, G., Anderson, A., Svec, H., 1973. A secondary isotopic standard for $^6\text{Li}/^7\text{Li}$ determinations. *International Journal of Mass Spectrometry and Ion Physics* 12, 265-272.
- Fryirs, K.A., Brierley, G.J., 2013. *Geomorphic analysis of river Systems: an approach to reading the landscape*. John Wiley & Sons.
- Gaillardet, J., Dupré, B., Louvat, P., Allègre, C.J., 1999. Global silicate weathering and CO_2 consumption rates deduced from the chemistry of large rivers. *Chemical Geology* 159, 3-30.
- Hinkle, S.R., 1996. Age of ground water in basalt aquifers near Spring Creek National Fish Hatchery, Skamania County, Washington, in: Fish, U.S., Wildlife, S., Geological, S. (Eds.), *Water-resources investigations report U.S. Dept. of the Interior, U.S. Geological Survey*.
- Huh, Y., Chan, L.H., Edmond, J.M., 2001. Lithium isotopes as a probe of weathering processes: Orinoco River. *Earth and Planetary Science Letters* 194, 189-199.
- Huh, Y., Chan, L.H., Zhang, L., Edmond, J.M., 1998. Lithium and its isotopes in major world rivers: Implications for weathering and the oceanic budget. *Geochimica et Cosmochimica Acta* 62, 2039-2051.
- Kisakürek, B., James, R.H., Harris, N.B.W., 2005. Li and $\delta^7\text{Li}$ in Himalayan rivers: Proxies for silicate weathering? *Earth and Planetary Science Letters* 237, 387-401.

- Kisakürek, B., Widdowson, M., James, R.H., 2004. Behaviour of Li isotopes during continental weathering: the Bidar laterite profile, India. *Chemical Geology* 212, 27-44.
- Kohn, M.J., Miselis, J.L., Fremd, T.J., 2002. Oxygen isotope evidence for progressive uplift of the Cascade Range, Oregon. *Earth and Planetary Science Letters* 204, 151-165.
- Liu, X.-M., Rudnick, R.L., 2011. Constraints on continental crustal mass loss via chemical weathering using lithium and its isotopes. *Proceedings of the National Academy of Sciences of the United States of America* 108, 20873-20880.
- Liu, X.-M., Rudnick, R.L., Hier-Majumder, S., Sirbescu, M.-L.C., 2010. Processes controlling lithium isotopic distribution in contact aureoles: A case study of the Florence County pegmatites, Wisconsin. *Geochemistry Geophysics Geosystems* 11, Q08014, 08010.01029/02010gc003063.
- Liu, X.-M., Rudnick, R.L., McDonough, W.F., Cummings, M.L., 2013. Influence of chemical weathering on the composition of the continental crust: Insights from Li and Nd isotopes in bauxite profiles developed on Columbia River Basalts. *Geochimica et Cosmochimica Acta* 115, 73-91.
- Magna, T., Wiechert, U.H., Halliday, A.N., 2004. Low-blank isotope ratio measurement of small samples of lithium using multiple-collector ICPMS. *International Journal of Mass Spectrometry* 239, 67-76.
- Marschall, H.R., Pogge von Strandmann, P.A.E., Seitz, H.-M., Elliott, T., Niu, Y., 2007. The lithium isotopic composition of orogenic eclogites and deep subducted slabs. *Earth and Planetary Science Letters* 262, 563-580.
- Millot, R., Vigier, N., Gaillardet, J., 2010. Behaviour of lithium and its isotopes during weathering in the Mackenzie Basin, Canada. *Geochimica et Cosmochimica Acta* 74, 3897-3912.
- Misra, S., Froelich, P.N., 2012. Lithium Isotope History of Cenozoic Seawater: Changes in Silicate Weathering and Reverse Weathering. *Science* 335, 818-823.
- Négre, P., Millot, R., Brenot, A., Bertin, C., 2010. Lithium isotopes as tracers of groundwater circulation in a peat land. *Chemical Geology* 276, 119-127.
- Nesbitt, H.W., Wilson, R.E., 1992. Recent chemical weathering of basalts. *American Journal of Science* 292, 740-777.
- Piper, A.M., 1953. A graphic procedure in the geochemical interpretation of water analysis. U.S. Dept. of the Interior, Geological Survey, Water Resources Division, Ground Water Branch, Washington.
- Pistiner, J.S., Henderson, G.M., 2003. Lithium-isotope fractionation during continental weathering processes. *Earth and Planetary Science Letters* 214, 327-339.
- Pogge von Strandmann, P.A.E., Burton, K.W., James, R.H., van Calsteren, P., Gislason, S.R., 2010. Assessing the role of climate on uranium and lithium isotope behaviour in rivers draining a basaltic terrain. *Chemical Geology* 270, 227-239.
- Pogge von Strandmann, P.A.E., Burton, K.W., James, R.H., van Calsteren, P., Gislason, S.R., Mokadem, F., 2006. Riverine behaviour of uranium and lithium isotopes in an actively glaciated basaltic terrain. *Earth and Planetary Science Letters* 251, 134-147.
- Qiu, L., Rudnick, R.L., Ague, J.J., McDonough, W.F., 2011a. A lithium isotopic study of sub-greenschist to greenschist facies metamorphism in an accretionary prism, New Zealand. *Earth and Planetary Science Letters* 301, 213-221.

- Qiu, L., Rudnick, R.L., McDonough, W.F., Bea, F., 2011b. The behavior of lithium in amphibolite- to granulite-facies rocks of the Ivrea–Verbano Zone, NW Italy. *Chemical Geology* 289, 76-85.
- Qiu, L., Rudnick, R.L., McDonough, W.F., Merriman, R.J., 2009. Li and $\delta^7\text{Li}$ in mudrocks from the British Caledonides: Metamorphism and source influences. *Geochimica et Cosmochimica Acta* 73, 7325-7340.
- Rudnick, R.L., Tomascak, P.B., Njo, H.B., Gardner, L.R., 2004. Extreme lithium isotopic fractionation during continental weathering revealed in saprolites from South Carolina. *Chemical Geology* 212, 45-57.
- Singleton, M.J., Sonnenthal, E.L., Conrad, M.E., DePaolo, D.J., Gee, G.W., 2005. Multiphase reactive transport modeling of seasonal infiltration events and stable isotope fractionation in unsaturated zone pore water and vapor at the Hanford site. *Vadose Zone Journal* 3, 775-785.
- Sonnenthal, E., Spycher, N., Apps, J., Simmons, A., 1998. Thermo-hydro-chemical predictive analysis for the Drift-Scale Heater Test. Yucca Mountain Project Level 4.
- Takeuchi, A., Hren, M.T., Smith, S.V., Chamberlain, C.P., Larson, P.B., 2010. Pedogenic carbonate carbon isotopic constraints on paleoprecipitation: Evolution of desert in the Pacific Northwest, USA, in response to topographic development of the Cascade Range. *Chemical Geology* 277, 323-335.
- Taylor, A.S., Lasaga, A.C., 1999. The role of basalt weathering in the Sr isotope budget of the oceans. *Chemical Geology* 161, 199-214.
- Teng, F.Z., McDonough, W.F., Rudnick, R.L., Dalpe, C., Tomascak, P.B., Chappell, B.W., Gao, S., 2004. Lithium isotopic composition and concentration of the upper continental crust. *Geochimica et Cosmochimica Acta* 68, 4167-4178.
- Teng, F.Z., McDonough, W.F., Rudnick, R.L., Wing, B.A., 2007. Limited lithium isotopic fractionation during progressive metamorphic dehydration in metapelites: A case study from the Onawa contact aureole, Maine. *Chemical Geology* 239, 1-12.
- Vigier, N., Gislason, S.R., Burton, K.W., Millot, R., Mokadem, F., 2009. The relationship between riverine lithium isotope composition and silicate weathering rates in Iceland. *Earth and Planetary Science Letters* 287, 434-441.
- Wanner, C., Sonnenthal, E.L., 2013. Assessing the control on the effective kinetic Cr isotope fractionation factor: A reactive transport modeling approach. *Chemical Geology* 337, 88-98.
- Wanner, C., Sonnenthal, E.L., Liu, X.-M., 2014. Seawater $\delta^7\text{Li}$: A direct proxy for global CO₂ consumption by continental silicate weathering? *Chemical Geology* 381, 154-167.
- Wimpenny, J., Gislason, S.R., James, R.H., Gannoun, A., Pogge Von Strandmann, P.A.E., Burton, K.W., 2010a. The behaviour of Li and Mg isotopes during primary phase dissolution and secondary mineral formation in basalt. *Geochimica et Cosmochimica Acta* 74, 5259-5279.
- Wimpenny, J., James, R.H., Burton, K.W., Gannoun, A., Mokadem, F., Gislason, S.R., 2010b. Glacial effects on weathering processes: New insights from the elemental and lithium isotopic composition of West Greenland rivers. *Earth and Planetary Science Letters* 290, 427-437.

Table 1. Sample locations, field measurements, major and trace element concentrations and Li isotopic compositions in dissolved and suspended loads of rivers.

2010 summer	units	Cameron	Milton	N. Scapoose	Silva	Deschutes	John Day	Hay	Wenas	Cowiche	Ahtanum	Mill	Asotin
Sample #		R1	R2	R3	R4	R5	R6	R7	R8	R9	R10	R12	R13
Longitude	°	-123.16707	-122.84415	-122.91550	-121.26745	-120.90903	-120.65085	-120.31797	-120.79715	-120.82127	-120.90663	-118.11638	-117.29242
Latitude	°	46.20735	45.86973	45.79293	45.71217	45.63033	45.72850	45.47992	46.89620	46.66437	46.51642	46.00358	46.27363
Location*		west	west	west	east	east	east	east	east	east	east	east	east
T	°C	15.6	18.6	15.2	18.1	19.2	21.9	19.6	12.6	18.8	14.6	14.1	18.1
pH		7.2	7.7	7.9	8.0	8.7	8.5	7.8	7.9	8.0	7.8	7.8	8.1
Conductivity	µS/cm	21	64	65	130	120	160	310	95	88	65	74	82
TDS	mg/l	10	32	32	64	58	82	150	47	44	32	35	41
Na	mg/l	2.7	4.9	5.3	6.5	9.6	7.0	17	3.9	4.0	3.2	3.8	3.5
Mg	mg/l	0.8	2.1	1.9	5.4	4.7	5.9	11	4.5	3.8	2.7	2.5	3.1
Al	µg/l	30	12	22	6.5	6.1	4.7	1.8	9.1	15	10	6.5	20
Si	mg/l	6.5	17	22	31	20	14	41	29	32	27	29	30
K	mg/l	0.4	1.1	1.3	1.5	1.7	1.4	3.7	1.6	2.1	1.8	2.3	2.3
Ca	mg/l	1.7	4.9	5.2	11	6.8	16	28	8.9	7.9	6.3	6.6	8.0
Fe	µg/l	130	320	170	28	21	32	54	130	180	79	50	35
F ⁻	mg/l	0.06	0.08	0.04	0.56	-	0.13	0.13	0.04	0.06	0.03	0.07	0.08
Cl ⁻	mg/l	2.6	4.0	18	54	13	8.5	8.6	16	13	16	3.2	2.8
NO ₃ ⁻	mg/l	-	-	-	-	-	-	0.01	-	-	0.01	-	-
SO ₄ ²⁻	mg/l	2.1	4.7	5.5	39	1.3	4.3	18	2.7	1.4	5.1	3.4	1.9
HCO ₃ ⁻	mg/l	0.9	0.9	1.3	1.0	1.5	2.7	-0.4	0.6	1.1	0.9	0.9	1.5
Li _{dis}	µg/l	0.1	0.7	1.6	0.4	4.7	1.6	3.2	0.7	1.1	0.7	0.9	1.0
δ ⁷ Li _{dis}		21.1	22.1	14.9	30.4	12.2	16.6	20.0	20.2	17.0	13.0	10.6	9.3
Li _{sus}	µg/g	-	-	14	-	7.5	15	-	24	-	-	-	7.2
δ ⁷ Li _{sus}		-	-	-5.6	-	4.2	-1.6	-	-3.1	-	-	-	-4.2

Note: “*” location relative to the Cascades (west or east). “-” under detection limit.

Table 1. Sample locations, field measurements, major and trace element concentrations and Li isotopic compositions in dissolved and suspended loads of rivers continued.

2012 winter	units	Cameron	Milton	N. Scapoose	Silva	Deschutes	John Day	Hay	Wenas	Cowiche	Ahtanum	Mill	Asotin	Mosquito
Sample #		R1	R2	R3	R4	R5	R6	R7	R8	R9	R10	R12	R13	R11
Longitude	°	-123.16707	-122.84415	-122.91550	-121.26745	-120.90903	-120.65085	-120.31797	-120.79715	-120.82127	-120.90663	-118.11638	-117.29242	-123.06510
Latitude	°	46.20735	45.86973	45.79293	45.71217	45.63033	45.72850	45.47992	46.89620	46.66437	46.51642	46.00358	46.27363	46.20202
Location*		west	west	west	east	east	east	east	east	east	east	east	east	west
T	°C	5.8	6.0	5.2	5.6	8.0	6.9	9.0	1.4	2.2	2.9	4.3	5.2	5.6
pH		6.7	6.9	8.3	7.6	8.0	7.7	7.8	7.6	7.6	7.6	7.4	7.6	6.7
Conductivity	µS/cm	14	31	37	65	110	130	320	97	100	91	51	74	20
TDS	mg/l	7	16	18	33	52	62	160	48	51	44	25	37	10
Na	mg/l	2.2	3.1	3.2	4.2	8.2	5.6	16	4.0	4.6	3.9	3.1	2.9	2.4
Mg	mg/l	0.6	1.0	1.0	2.7	4.0	4.4	10	4.3	4.4	3.6	1.7	2.7	0.8
Al	µg/l	16	4.9	8.9	86	43	40	2.1	57	23	22	180	240	12
Si	mg/l	4.1	9.2	12	21	22	19	34	27	30	30	24	27	4.8
K	mg/l	0.3	0.6	0.8	0.9	1.5	1.3	3.8	1.5	1.9	2.0	1.5	1.7	0.3
Ca	mg/l	1.6	2.8	3.1	6.3	6.4	12	27	8.6	8.8	7.9	4.8	6.9	1.9
Fe	µg/l	20	14	16	55	34	51	57	93	76	55	220	250	37
F ⁻	mg/l	0.01	0.02	0.03	0.04	0.10	0.08	0.42	0.09	0.10	0.07	0.15	0.08	0.01
Cl ⁻	mg/l	3.3	2.6	2.9	1.6	1.8	1.2	11	0.4	0.9	0.4	0.5	0.7	2.7
NO ₃ ⁻	mg/l	2.0	3.3	2.8	0.0	0.4	0.3	1.5	0.0	0.0	0.0	0.2	0.3	4.8
SO ₄ ²⁻	mg/l	0.5	1.2	1.6	0.7	1.8	3.9	15	2.0	3.2	1.6	0.6	1.3	0.5
HCO ₃ ⁻	mg/l	0.6	0.4	0.7	2.5	2.6	2.6	3.9	1.7	1.8	3.1	7.2	9.6	0.6
Li _{dis}	µg/l	0.1	0.4	0.9	0.3	3.5	1.1	2.9	0.5	1.1	0.8	0.7	0.7	0.2
δ ⁷ Li _{dis}		17.4	13.0	8.8	14.0	12.5	13.5	18.8	21.6	16.1	13.1	10.9	8.9	15.9
Li _{sus}	µg/g	16	20	66	18	13	20	21	24	16	16	19	36	17
δ ⁷ Li _{sus}		-1.4	-2.5	-4.5	-0.9	-0.3	-1.5	-0.2	-3.1	-5.7	-5.9	-2.8	-5.2	-1.0

Note: “*” location relative to the Cascades (west or east). “-” under detection limit.

Table 2. Sample locations, field measurements, major and trace element concentrations and Li isotopic compositions of groundwaters and one alkaline lake.

Groundwater	units	Spring Creek	Selah	Ryegrass	Lind	Hatton	Soap Lake
Sample #		G1	G2	G3	G4	G5	L1
Longitude	°	-121.54613	-120.44327	-120.20900	-118.62250	-118.74282	-119.49877
Latitude	°	45.72737	46.69758	46.94738	46.96828	46.79410	47.42263
Sampling*		well	faucet	faucet	well	faucet	
T	°C	17.6	18.1	14.7	28.6	10.9	10.2
pH		8.8	8.0	7.7	9.1	7.9	9.6
Conductivity	µS/cm	180	320	340	350	510	> 3999
TDS	mg/l	90	160	170	180	250	>2000
Na	mg/l	33	21	13	78	19	280
Mg	mg/l	0.4	12	15	0.3	19	4.4
Al	µg/l	6.9	27	0.5	4.9	0.1	-
Si	mg/l	45	33	40	64	35	4.9
K	mg/l	4.5	3.9	2.9	3.9	4.0	590
Ca	mg/l	1.9	17	19	3.1	40	6.9
Fe	µg/l	47	6.9	5.7	17	54	1.3
F ⁻	mg/l	0.76	0.48	0.39	3.3	0.28	0.31
Cl ⁻	mg/l	3.6	8.6	7.0	7.9	46	130
NO ₃ ⁻	mg/l	0.01	-	11	0.1	18	-
SO ₄ ²⁻	mg/l	1.5	3.7	12	4.7	50	210
HCO ₃ ⁻	mg/l	3.5	1.8	2.4	2.4	3.4	-0.87
Li _{dis}	µg/l	21	9.8	6.5	8.9	3.3	1.5
δ ⁷ Li _{dis}		6.8	8.1	9.4	21.4	6.7	20.5

Note: “*” sampling methods (well or faucet). “-” below detection limit.

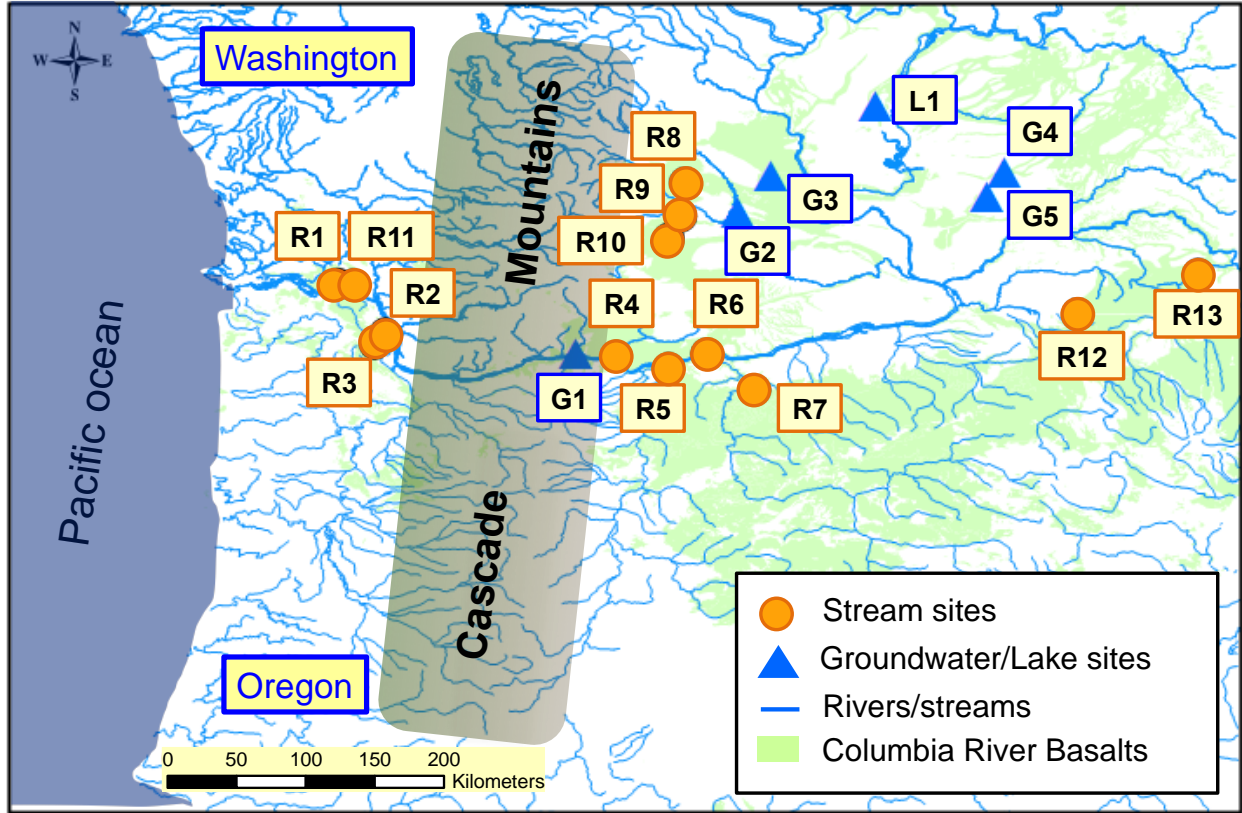


Figure 1. Map of sample locations. Geological data are from USGS. Streams are shown in orange circles and numbered with Rx. R11 was only sampled during late winter of 2012 and the rest rivers were sampled both in summer of 2010 and late winter of 2012. Groundwater and one lake are shown in blue triangles, all of which were sampled during late winter.

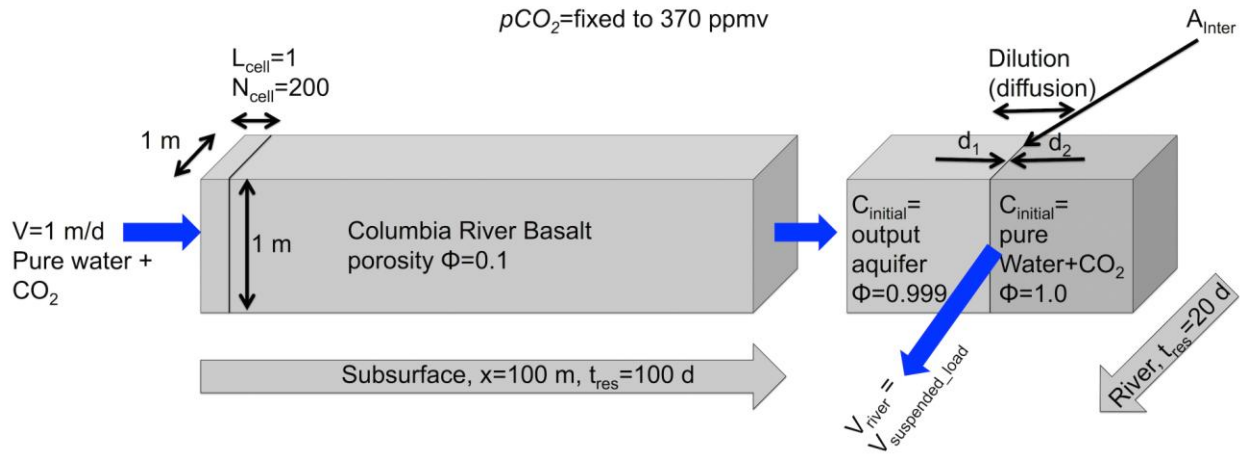
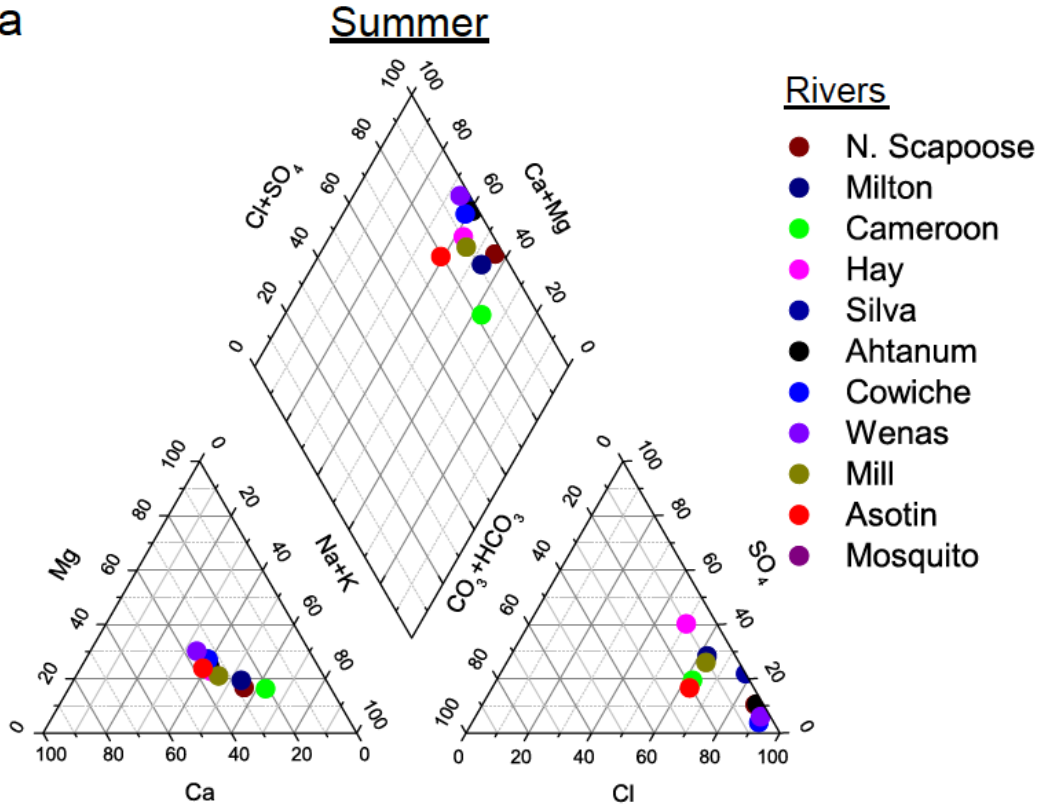


Figure 2: Model setup illustrating that simulations were run for a 100 m long aquifer exfiltrating into a river system, eventually. River simulations were run as batch simulations (no flow) assuming that the suspended load is transported at the same velocity as river water. Moreover, river simulations consider a diffusive dilution of the exfiltrated groundwater with water that experienced no previous water-rock interaction (i.e., pure water+CO₂). For both systems (aquifer and river), Li isotope fractionation is simulated to occur during hematite and kaolinite precipitation.

a



b

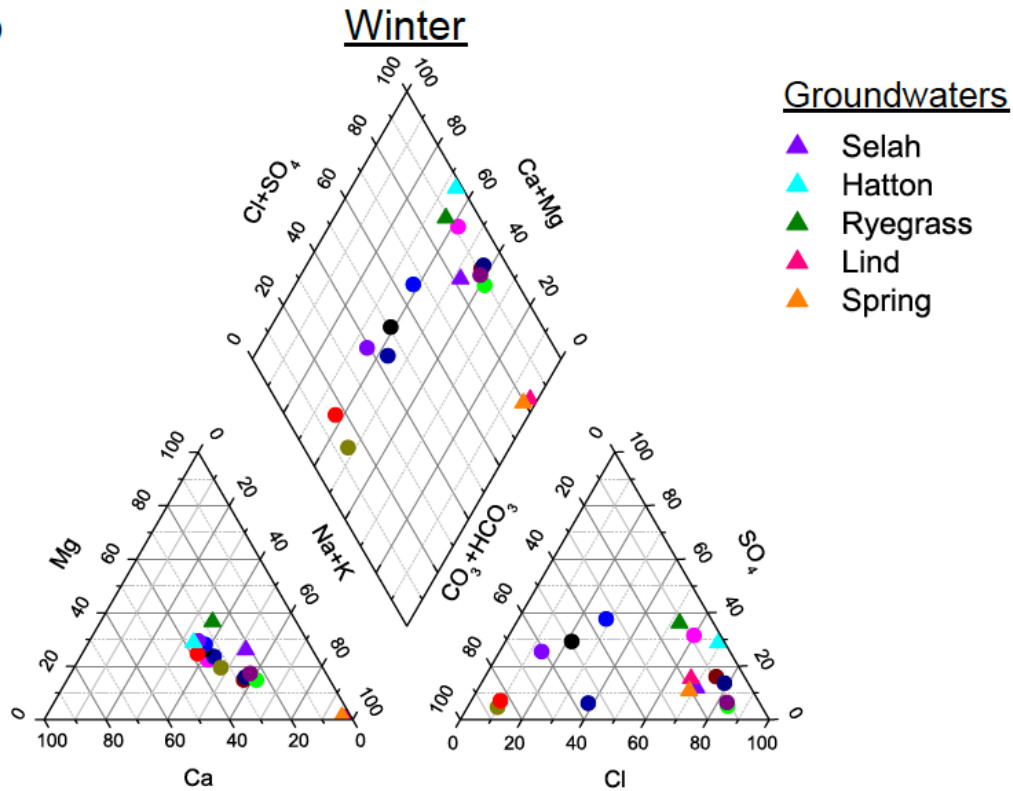


Figure 3. Piper diagram (Piper, 1953) of streams and groundwaters in summer (a) and late winter (b). Stream waters and groundwaters are shown in circles and triangles, respectively.

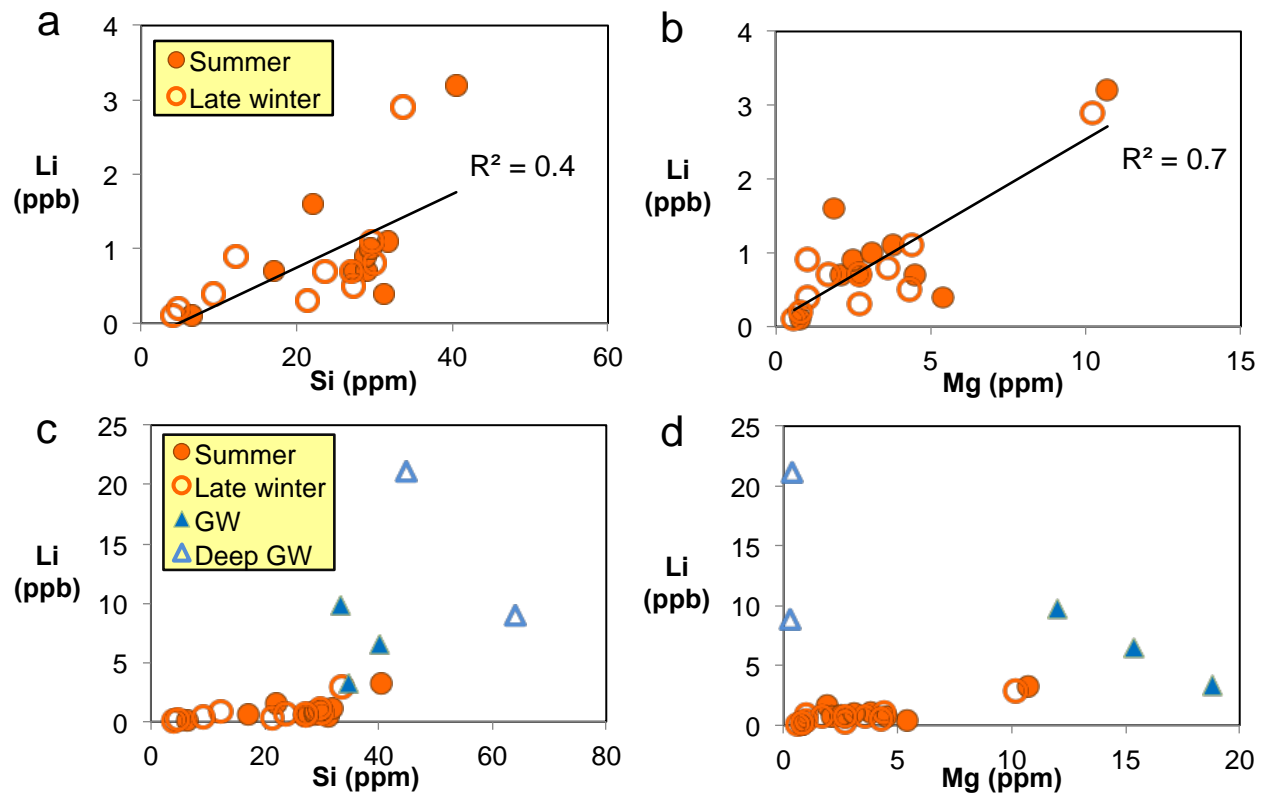


Figure 4. Plots of [Li] versus [Si] and [Mg] in streams and groundwaters. Summer and late winter stream waters are shown in open and closed orange circles, respectively. Groundwaters feeding the streams are in solid blue triangles, deep seated and ancient groundwaters are shown in open blue symbols.

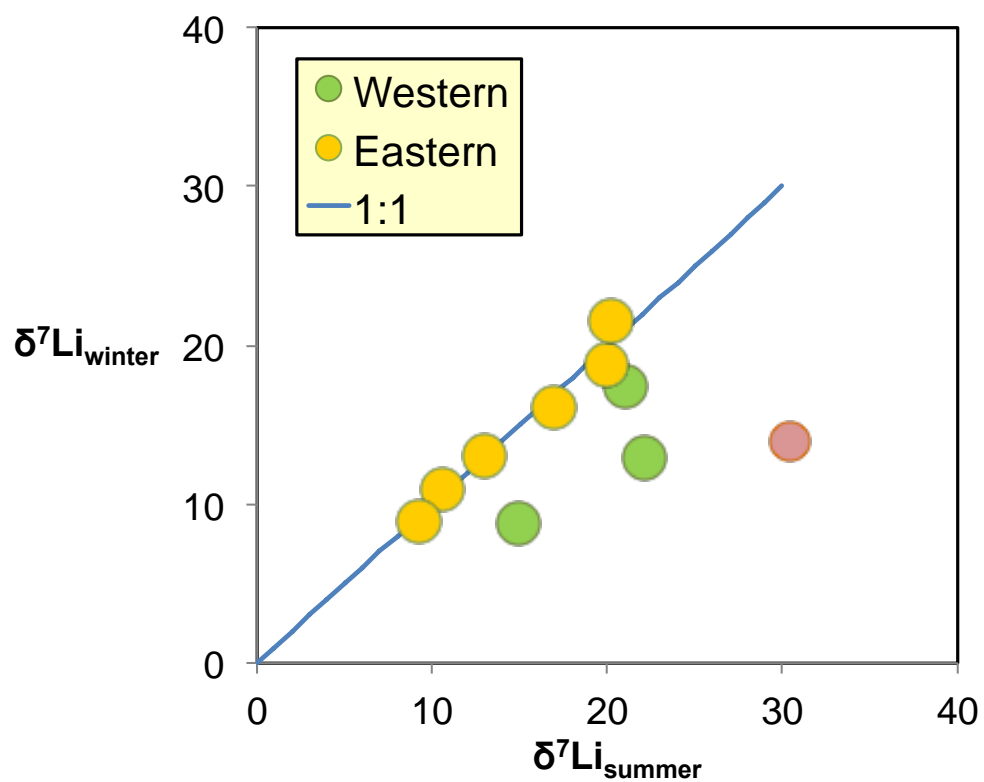


Figure 5. $\delta^7\text{Li}_{\text{dis}}$ in summer vs. winter for western and eastern streams. The sample showing suspected anthropogenic contamination (Silva, eastern) is plotted as a red circle (see main text for details).

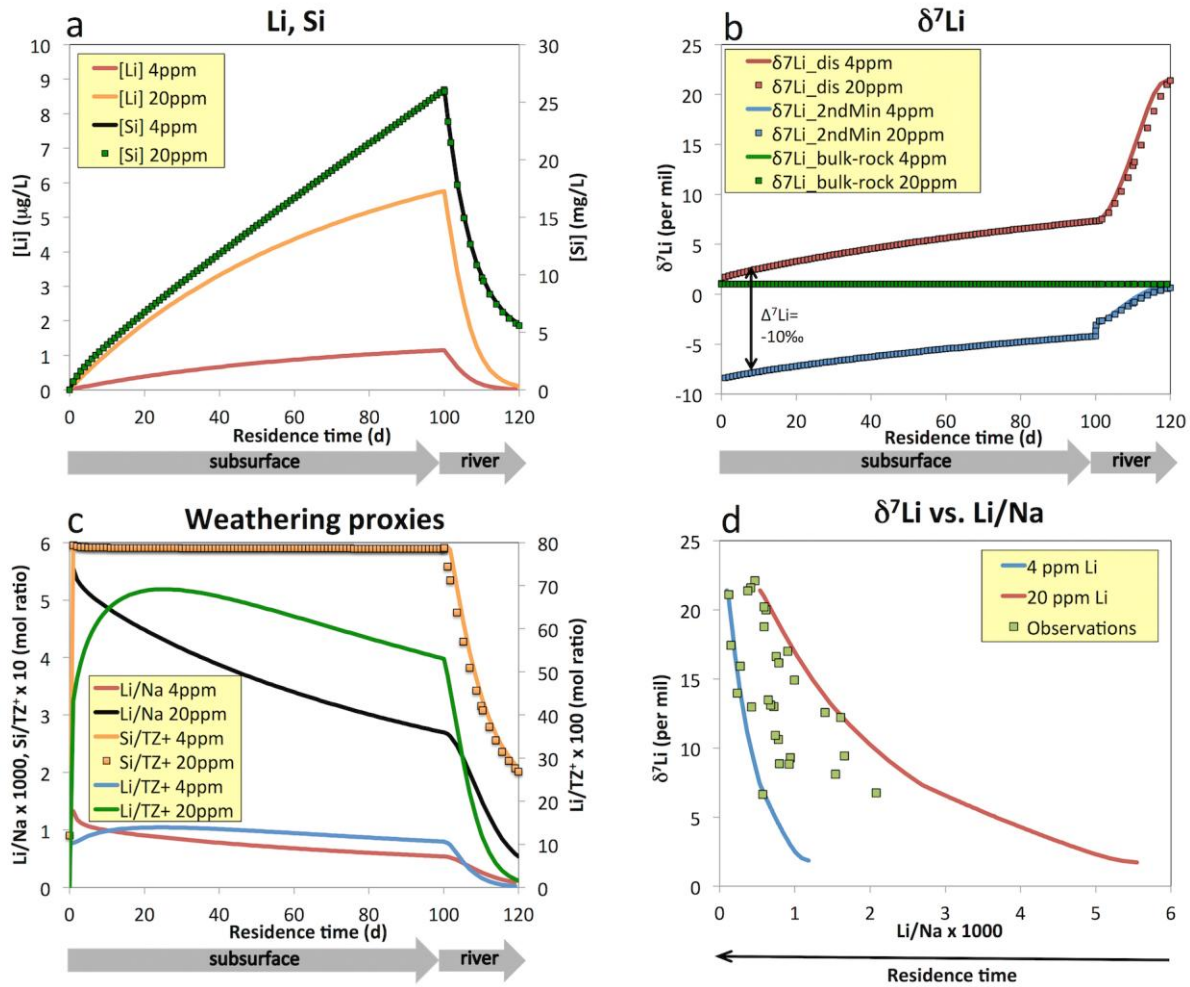


Figure 6: Model results for initial CRB Li concentrations of 4 ppm and 20 ppm. a illustrates steady state Li and Si concentration profiles along the full model domain (subsurface + river). b presents corresponding steady-state $\delta^7\text{Li}$ profiles for aqueous Li ($\delta^7\text{Li}_{\text{dis}}$), Li in precipitating secondary clays ($\delta^7\text{Li}_{\text{kaolinite}} = \delta^7\text{Li}_{\text{hematite}}$ summarized as $\delta^7\text{Li}_{\text{2ndMin}}$) and Li of the bulk solid. c illustrates steady state profiles of typical silicate weathering tracers such as Si/TZ^+ , Li/TZ^+ and Li/Na . d Comparison between the simulated $\delta^7\text{Li}$ vs. Li/Na relation (curves) and the one observed in groundwaters and streams draining the Columbia River Basalt (Tables 1 and 2). Decreasing Li/Na ratio reflects increasing subsurface and/or river residence time. All profiles are plotted against fluid residence time to simultaneously illustrate subsurface and river simulations. In the subsurface domain, fluid residence time (x-axis) also corresponds to the distance along the subsurface domain because the flow velocity was 1 m/d.

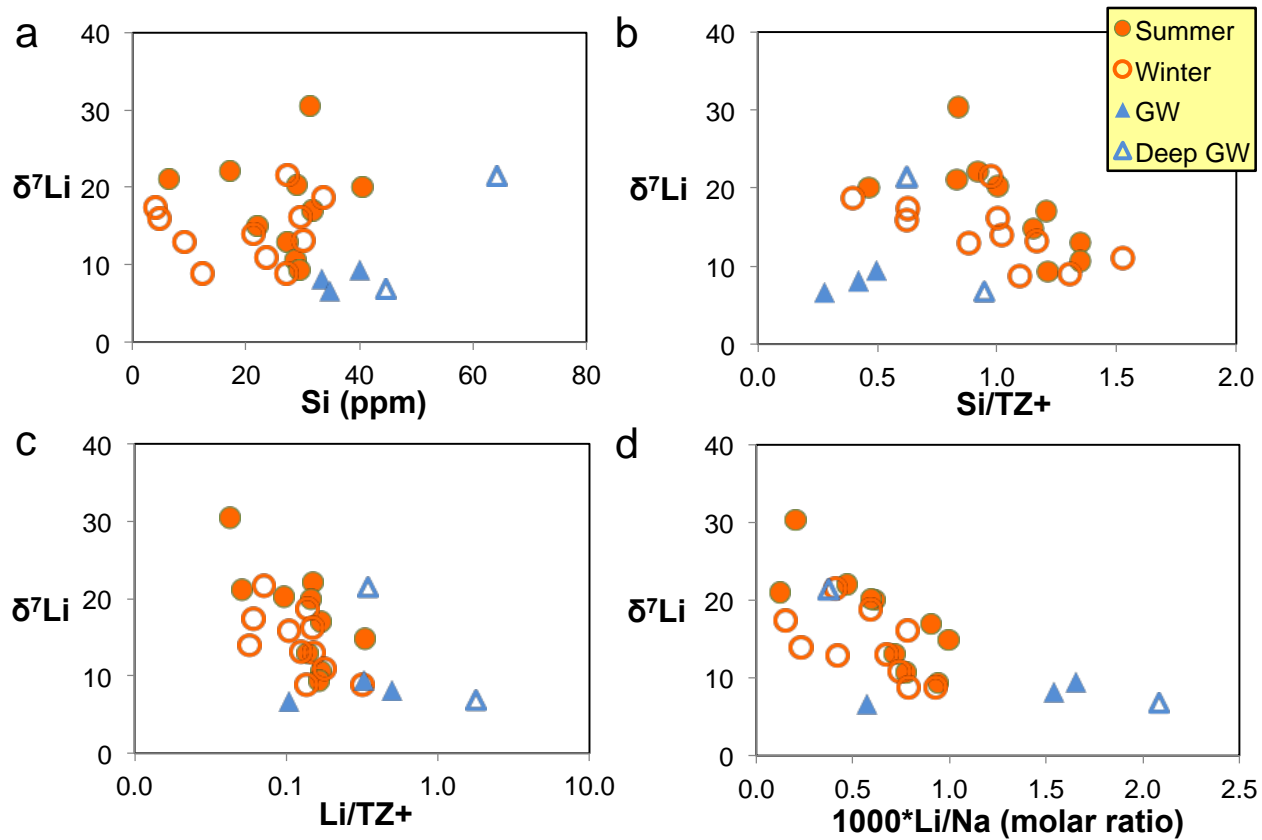


Figure 7. $\delta^7\text{Li}_{\text{dis}}$ versus [Si], Si/TZ^+ , Li/TZ^+ , and $1000 \times \text{Li}/\text{Na}$ (molar ratio) in stream waters and groundwaters. Summer and late winter stream waters are shown in open and closed orange circles, respectively. Groundwaters feeding streams are in solid blue triangles, deep-seated groundwaters are in open blue triangles. The total cation charge (TZ^+) is defined as $\text{TZ}^+ = \text{Na}^+ + 2\text{Mg}^{2+} + \text{K}^+ + 2\text{Ca}^{2+}$ in 10^{-3} equivalents per liter, mEq/L.

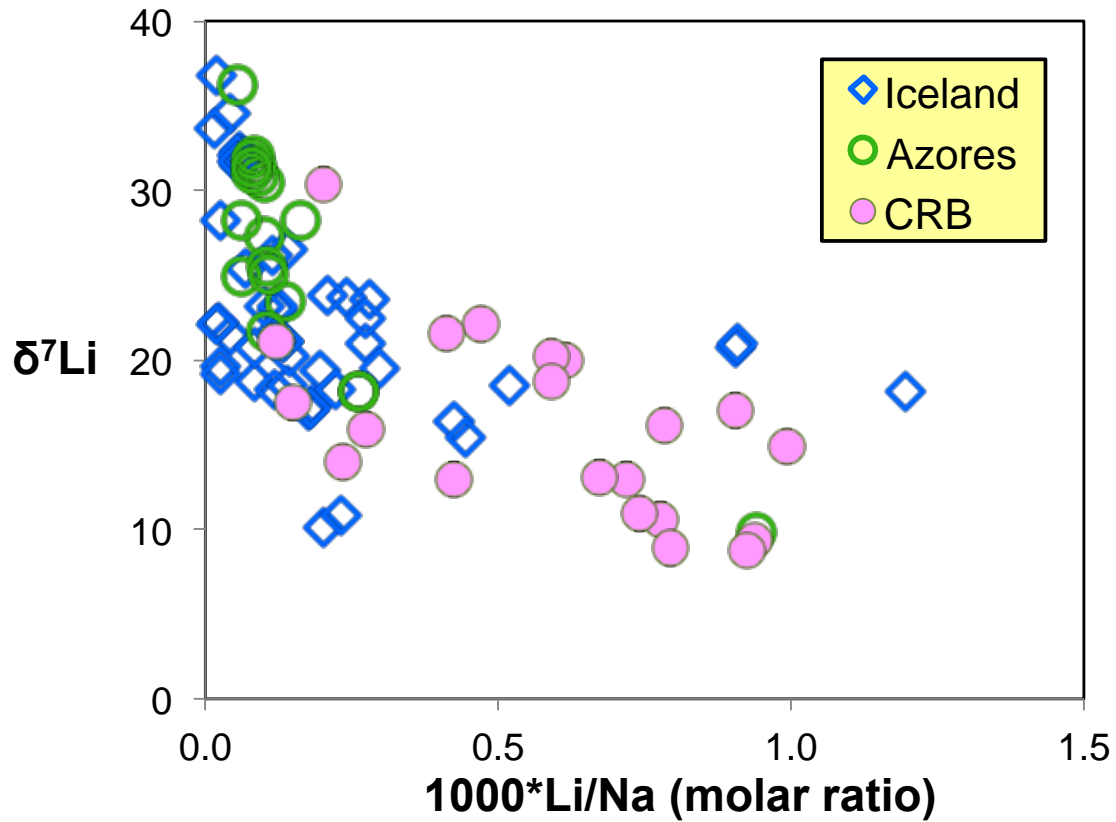


Figure 8. $\delta^7\text{Li}$ versus $1000 \times \text{Li}/\text{Na}$ (molar ratio) in dissolved loads of streams and rivers draining basalts. Data are from this study, Pogge von Strandmann et al. (2006; 2010), and Vigier et al. (2006; 2009).